Sustainable Energy & Fuels



PAPER

View Article Online
View Journal | View Issue



Cite this: Sustainable Energy Fuels, 2021. 5. 5257

Ultrathin alumina passivation for improved photoelectrochemical water oxidation catalysis of tin oxide sensitized by a phosphonate-functionalized perylene diimide first without, and then with, CoO_v †

Carly F. Jewell, ¹ Ashwanth Subramanian, ¹ Chang-Yong Nam ¹ ** Chang-Yong Nam ¹

Previously, a photoanode composed of nanostructured SnO₂ coated with the perylene diimide dye N,N'bis(phosphonomethyl)-3,4,9,10-perylenediimide (PMPDI) plus photoelectrochemically deposited cobalt oxide (CoO_v) was shown to photoelectrochemically oxidize water at 31 \pm 7% faradaic efficiency. A nonideal part of that prior system is that the addition of the known CoO, water oxidation catalyst (WOC) resulted in a reduction of the total photocurrent rather than the anticipated increase, due to an increase in charge-carrier recombination. Herein, we show deposition of an ultrathin alumina overlayer applied by atomic layer deposition (ALD) on the SnO₂/PMPDI photoanode can improve the photoactivity and catalytic activity of the system; the addition a ca. 1 nm-thick AlO_x layer deposited on a 4000 nm (i.e., 4 micron) thick mesoporous anode system can and does have a positive, 2.5-fold improvement in the steady-state photocurrent with 29 \pm 9% faradaic efficiency vs. the control anode without alumina passivation by reducing charge-carrier recombination. Moreover, ALD-deposited AlO_x layer does help support the understanding of the "anti-catalysis" of co-depositing a CoO_y WOC on the SnO_2 /PMPDI DS-PECs-specifically the picture of direct CoO_v-SnO₂ contact-mediated recombination-but that AlO_x layer was unable to improve the photocurrent in a net SnO₂/PMPDI/AlO_x(/CoO_y) system. We attribute the lack of a performance enhancement by CoO_v WOC to incomplete coverage of each SnO₂ nanoparticle by the AlO_x. Overall, we find the addition of an optimized ultrathin AlO_x layer (0.6 nm thick; deposited at 85 °C) improves the SnO₂/PMPDI/AlO_x system's photoactivity by a factor of up to ca. 3-fold with reduced recombination. These results document that metal-oxide passivation by low-temperature ALD can be an effective strategy for improving the water oxidation performance of even nanostructured dve sensitized-photoelectrochemical cell.

Received 17th June 2021 Accepted 1st September 2021

DOI: 10.1039/d1se00908g

Introduction

Efficient photoelectrochemical solar water splitting into molecular hydrogen and oxygen is one of the must-solve problems in chemistry 1,2 en route to fulfilling the growing global demand for clean, renewable energy while minimizing $\rm CO_2$ emissions. $^{3-7}$ Recently, the application of organic dyes as light absorber for solar water splitting has drawn extensive attention

due to their relatively low cost, their production from earthabundant materials, the ease of processability, and the ability to synthetically tailor the organic dye as needed en route to optimized water-splitting performance.^{4,8} Previously, we developed a first,⁹ then a second¹⁰ generation water-oxidation photoanode using both organic thin-film and dye-sensitized photoelectrolysis cell (OTF-PEC and DS-PEC) architectures

[†] Electronic supplementary information (ESI) available. See DOI: 10.1039/d1se00908g

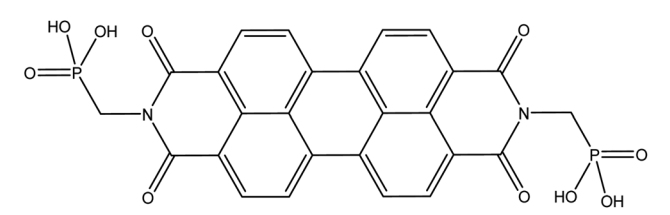


Fig. 1 Molecular structure of PMPDI.

^aDepartment of Chemistry, Colorado State University, Fort Collins, Colorado, 80523, USA. E-mail: Richard.Finke@colostate.edu

^bCenter for Functional Nanomaterials, Brookhaven National Laboratory, Upton, New York 11973, USA. E-mail: cynam@bnl.gov

Department of Materials Science and Chemical Engineering, Stony Brook University, Stony Brook, New York 11794, USA

based on a perylene diimide dye derivative (N,N'bis(phosphonomethyl)-3,4,9,10-perylenediimide, PMPDI, Fig. 1) and a co-deposited CoO_v water oxidation catalyst (WOC).11-13 Perylene diimides (PDIs) have high light-absorption extinction coefficients (ca. 22 000 M⁻¹ cm⁻¹ at λ_{max} of 500 nm for PMPDI¹⁰) and are used in industrial settings as both car paints and in plastics.8 PDIs are further attractive as the lightgathering component in water-oxidation catalysis (WOCatalysis) devices due to their high thermal stability,14 high oxidative stability both in air and in water, and due to their resistance to photobleaching under even extreme conditions, including hypochlorite solutions.15

As for the WOC component, CoO_v is an earth-abundant, heterogeneous, prototype WOC.16 Our previous study on the PMPDI OTF-PEC architecture showed a 10-fold enhancement of water-oxidation photocurrent by applying co-deposited CoO_v as the WOC,9 but the system exhibits a low light-harvesting efficiency (LHE) (ca. 12% at $\lambda_{max}\!)$ and a large amount of charge carrier recombination, yielding only a 6% charge transport efficiency.9 An optimized second-generation PMPDI DS-PEC system architecture consisting of nanostructured SnO2 coated with PMPDI is able to achieve a LHE of >99% at λ_{max} and a charge transport efficiency of 13%.10 However, it was found that the same CoO_v WOC, necessary to produce oxygen, in fact decreased the water oxidation performance in the secondgeneration SnO₂/PMPDI/CoO_v system relative to the first. 9,10 That unexpected, undesired, "anti-catalyst" behavior was attributed to increased charge recombination between photoinjected electrons in the SnO2 conduction band and accumulated holes in CoOy at the SnO2 surface. 10,17,18 More generally, that "anti-catalyst" behavior illustrates the acknowledged broader challenge19 of coupling water-oxidation as well as others catalysts to light-absorbing units in ways that minimizes charge-carrier recombination back reactions.

To begin to address the forefront question of how to best couple catalysts and light-adsorbing units, we previously attempted to improve the performance of SnO₂/PMPDI/CoO_y DS-PECs by using a wet chemical method¹⁰ to deposit a thin layer of electronic insulator AlOx on the SnO2 surface as an established tunneling barrier^{17,20} against recombination. That effort led to an improved photovoltage, but a reduced photocurrent due to a hindered charge injection between the dye and SnO2.10

In related work, Kamire et al. reported reduced charge recombination by applying 0.5-3 nm thick ultrathin AlOx coating directly over dyes by atomic layer deposition (ALD) in a DS-PEC system consisting of nano-TiO2 sensitized by perylene monoimide (PMI) dye.21 The observed decreased recombination was attributed to the passivation of recombination-active TiO₂ surface states and to an increased barrier for tunneling-based recombination with redox-active species in solution.21 The addition of the AlO_x layer further served to stabilize the dye, resulting in improved device lifetimes. Significantly, those workers observed that the addition of an Ir-dimer-based WOC resulted in a ca. 66% reduction of photocurrent, both with and without the AlO_x overlayer,²¹ closely analogous to what we have observed in our previous study where the addition of the known

WOC16 COO_v decreased the photocurrent output of SnO₂/PMPDI DS-PEC.¹⁰ These examples make apparent the forefront problem of effectively coupling the DS-PEC systems to desired catalysts such as a WOC without, instead, enhancing undesirable recombination. These studies further suggest the hypothesis that the performance of DS-PECs and catalysts may be improved if the recombination passivation layer can be further optimized to also allow the WOC to function as desired.

Herein, we explore the impact of adding an insulating AlO_x layer prepared by ALD onto PMPDI-sensitized nanostructured SnO₂ DS-PECs on their solar water splitting performance, idealized by Fig. 2. More specifically, we address five primary questions via the ALD approach: (i) can the deposition of an ultrathin alumina overlayer applied by ALD on the PMPDI/SnO₂ photoanode improve the photoactivity and catalytic activity of the CoO_v WOC? More specifically, (ii) can the addition of a 0.6 to 1.3 nm thickness AlO_x layer have any measurable, much less useful effect, on a 4000 nm (i.e., 4 micron) thick and also nanoporous anode system? If so, (iii) what are the effects of key parameters on the photo- and catalytic-activity, notably the layer thickness and deposition temperature of the alumina overlayer? (iv) Can a better, ALD-controlled deposition of an ultrathin AlO_r layer address the carrier recombination issues of SnO2/PMPDI DS-PECs, and (v) can the ultrathin, ALD-deposited AlOx layer probe, and perhaps even improve our understanding of why codeposited CoO_v WOC on the SnO₂/PMPDI DS-PECs has, to date, resulted in a decreased, "anti-catalysis" photocurrent? In the present study we investigate the effects of ultrathin AlO_r thickness (0.6-1.3 nm) and ALD temperature applied to a 4 µm thick DS-PEC photoanode system on the overall anode photoactivity, device/organic dye stability, and, importantly, on the catalytic activity of CoO_v WOC by characterizing the system's open-circuit photovoltage, photocurrent, and O₂ product yield and hence faradaic efficiency under solar PEC water splitting conditions. The results allow insights into the five questions

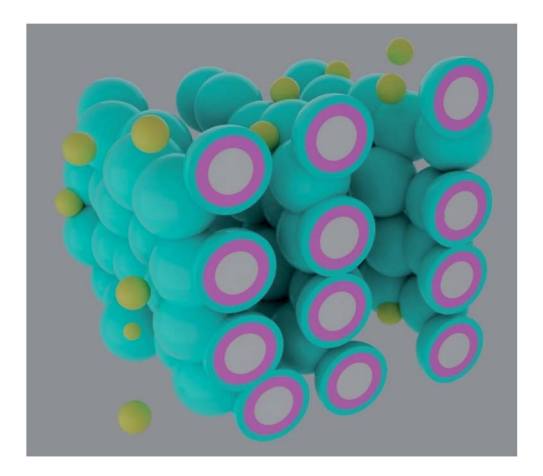


Fig. 2 Idealized structural models of the SnO₂/PMPDI/AlO_x/CoO_v anode where SnO₂ is grey, PMPDI is pink, AlO_x is blue, and CoO_y is yellow. Nanostructured SnO2 is reflective of SEM images that will be presented in a figure later in the paper. 10 Anode notation throughout is written in order of deposition, left to right (i.e. SnO₂ is deposited first, followed by PMPDI, then AlOx, and then finally CoOv).

posed that form the basis for the present research. In addition, the studies which follow make apparent when and how ALDdeposited alumina layers should or should not be used to try to improve analogous DS-PECs, the needed considerations of layer thickness, and factors to be considered when using ALD on nanostructured devises. The results provide a working hypothesis for going forward about how to couple WOC and other catalysts to DS-PECs for improved catalyst efficiency.

Experimental

Materials

The following starting materials and solvents were used as received to generate buffer solutions: KOH (Fisher, Certified ACS grade, 98.5%, 1.5% water, 0.00028% Fe, 0.0008% Ni); KH₂PO₄ (Fisher, Certified ACS Grade, 99.3%, 0.0005% Fe); hydroquinone (Aldrich, >99%); NANOpure water (Barnstead NANOpure ultrapure water system, 18.0 M Ω). NANOpure water was used for all experiments.

Synthesis of PMPDI dye, and the deposition of SnO₂ anode and CoO_v WOC

All synthetic and manufacturing details for PMPDI dye and the SnO₂ anodes can be found in our previous publications.^{9,10} Briefly, the anodes are composed of fluorine-doped tin oxide (FTO)-coated glass as a transparent current collector, covered by a mesoporous SnO₂ film, sensitized with PMPDI, and CoO_v WOC. All fabricated photoanodes have SnO2 film with "2-Scotch" layer thickness conditions on where PMPDI dyes were loaded for 24 h at 95 °C from a saturated solution of fully protonated PMPDI in water.10 CoO_v WOC was added to photoanodes by photoelectrochemical deposition;9,10 the anodes (SnO₂/PMPDI or SnO₂/PMPDI/AlO_x) were submerged in a solution of pH 7, 0.5 mM Co(NO₃)₂ and 0.1 M potassium phosphate butter (KPi) and held at +0.2 V vs. Ag/AgCl under 1 sun illumination for 3 min. 10 Anodes were then rinsed with water for 30 s and allowed to air dry.

Ultrathin AlO_x coating by ALD

Ultrathin conformal AlO_x layer was deposited on PMPDI or glass substrate using a Cambridge Nanotech Savannah S100 ALD system (base pressure ~ 0.4 Torr). The deposition temperature was set at 85 °C; PMPDI was shown to be stable up to 400 °C herein. The depositions were carried out by sequential exposure of trimethyl aluminum (TMA) (14 ms) and water vapor (40 ms) with an intermediate purge time of 60 s for both precursors. Spectroscopic ellipsometry was used to calibrate the AlO_x thickness per ALD cycle using Si control substrates and found a linear growth rate of 0.067 nm per cycle (Fig. S1 and Table S1; see ESI† for details). The number of ALD cycles was varied between 4 and 28 to deposit AlOx on SnO2/PMPDI or glass substrates ranging between 0.4 and 2.0 nm, respectively. In a separate set of experiments, the ALD temperature has been varied from 85, 150, and to 200 °C to investigate the impact of deposition temperature on the device performance. AlO_x deposition was verified using scanning electron microscopy

(SEM) imaging and X-ray photoelectron spectroscopy (XPS) methods, vide infra.

Photoelectrochemical testing

All photoelectrochemical experiments were done in a previously described10 custom two-compartment Pyrex cell consisting of a working compartment (1 \times 1.5 \times 1.5 cm³, 5 ml) and an auxiliary compartment separated by a medium porosity glass frit. Experiments were conducted using a CH Instruments CHI630D potentiostat, a Pt wire counter electrode positioned in the auxiliary compartment and a Ag/AgCl (3 M NaCl, +0.215 V vs. normal hydrogen electrode (NHE)) reference electrode positioned in the working compartment in close proximity to the anode surface. The anode was clamped with an alligator clip to the front wall of the working compartment with the uncoated, nonconductive glass side pressed against the cell wall. The cell was filled with ca. 5 ml electrolyte (pH 7, 0.1 M KPi buffer) sufficient to cover the film. The anode was illuminated from the substrate side using a 65 W xenon arc lamp (PTO model A1010), which was powered by an OLIS XL150 adjustable power supply. The light passed through a bandpass filter (315-710 nm, Thorlabs KG3, FGS900S) and an ultraviolet (UV) filter (400 nm long-pass, Thorlabs FGL400S). The power density of the light was adjusted to reflect the visible region of the airmass 1.5 global (AM 1.5G) spectrum.10 In the experiments in which transients (interrupted illumination) of 5 s or 30 s were used, a manual shutter was used to block the light.10 Each anode was tested with a series of electrochemical experiments in the order detailed below. First the cell was allowed to short-circuit in the dark for 60 s to depopulate the electrons from SnO2 subbandgap states.10 The 60 s was determined to be a sufficient length of time to depopulate the excited state as the current reached a steady-state within 15 s. Then the open-circuit potential, V_{oc} , was measured vs. the Ag/AgCl reference electrode for 90 s in the dark and then measured again under illumination for 90 s. Next, a photocurrent transient experiment was performed in which the anode was held at +0.2 V vs. Ag/ AgCl for 300 s with 30 s light/dark transients throughout. A potential of +0.2 V vs. Ag/AgCl was chosen for photocurrent transient experiments as photocurrent is fully saturated by this applied potential. The cell was again allowed to short-circuit in the dark for 60 s, and the $V_{\rm oc}$ in both the dark and light were remeasured. Then the current-voltage (i-V) photocurrent transient experiment was performed. The voltage was scanned from -0.2 to +1.0 V vs. Ag/AgCl with a 10 mV s⁻¹ scan rate and 5 s light transients. Each experiment was reproduced a minimum of three times with three separate anodes produced under identical conditions. All figures and values reported herein are representative of the photoactivity of the system indicated. Care was taken to ensure that the reported results are reproducible and not due to a defective anode or otherwise irreproducible sample.

IPCE and APCE determinations

Incident photon to current efficiency (IPCE) measurements were calculated from action spectra collected using a Xe arc lamp (Oriel model 66002, calibrated to approximate the AM1.5 reference power in the visible region), power supply (Oriel model 68700), monochromator (Oriel Cornerstone 130, model 7400), and a CH Instruments 630D potentiostat. All experiments were run in the presence of 20 mM H₂Q sacrificial agent in pH 7 0.1 M KPi buffer using the same two-compartment Pyrex cell used for all photoelectrochemical testing; a Pt wire counter electrode positioned in the auxiliary compartment and a Ag/AgCl (3 M NaCl, +0.215 V vs. normal hydrogen electrode (NHE)) reference electrode positioned in the working compartment in close proximity to the anode surface were again used. In order to collect the action spectra, the electrode being test was held at +0.2 V vs. Ag/AgCl while incident monochromatic light (ca. 3 nm bandwidth) was scanned from 400 to 700 nm across 25 nm intervals. A silicon standard power sensor (Thorlabs model S120B) was used to measure the incident lamp power through the same aperture at each wavelength, P_{mono} . Photocurrent, I_{ph} , was measured at each wavelength by recording the photocurrent during three 15 seconds light transients and subtracting off any dark current. The average photocurrent was then used to calculate the IPCE according to eqn (1):

IPCE (
$$\lambda$$
) = $\frac{I_{\text{ph}} \text{ (mA)} \times 1239.8 \text{ (V nm)}}{P_{\text{mono}}(\text{mW}) \times \lambda \text{ (nm)}}$ (1)

The absorbed-photon-to-current efficiency (APCE) was calculated by dividing the light harvesting efficiency (LHE)-i.e., the absorptance spectrum measured from the anode—out of the IPCE, using eqn (2). Note that the APCE is equivalent to the injection efficiency, $\phi_{\rm inj}$, multiplied by the charge collection efficiency, $\eta_{\rm col}$.

$$APCE = \frac{IPCE}{LHE} = \phi_{inj}\eta_{col}$$
 (2)

Oxygen detection

Oxygen yield was experimentally measured using the generatorcollector (G-C) technique detailed elsewhere:10,22-24 photoanode 'generators' were sandwiched with an FTO "collector", 10 separated by a Parafilm spacer. A CH Instruments CHI-750D bipotentiostat was used for the G-C experiments. The G-C cell was placed in the previously detailed working compartment with the generator side against the wall of the cell with the incoming light. The cell was filled with pH 7, 0.1 M KPi buffer, approximately 10 ml, which was degassed with Ar for a minimum of 30 min. An Ag/AgCl (3 M NaCl) electrode was used as a reference and was also placed in the working compartment. A Pt wire was used as a counter electrode and was placed in the auxiliary compartment. Current was measured at both the generator and collector electrodes, which were held at +0.2 V and -0.65 V vs. Ag/AgCl, respectively. The current was collected for 300 s in the dark, 300 s in the light, then 300 s in the dark in order to ensure that all oxygen had diffused across the two electrodes and that all current attributable to oxygen production was collected. Control experiments with FTO/CoO_v anodes were used to determine the collection efficiency of the sandwich configuration and used to calculate the O2 yield and faradaic efficiency of each photoanode.

Results and discussion

The effects of AlOx overlayer on the photoelectrochemical activity of SnO₂/PMPDI

As noted in the Introduction, the addition of an electronically insulating metal-oxide shell layer over the mesoporous semiconductor substrate (and sometimes the dye as well) has been shown to reduce recombination and increase photocurrents in dye-sensitized systems. 17,20,21,25-32 In a previous study, 1.3 nm thick metal oxide deposited at 85 °C was found to be optimal for a photoanode system based on organic semiconductor thin films.28 Hence, as to start and as a baseline, a 1.3 nm thick layer of AlO_x was deposited at 85 °C by ALD onto the previously optimized¹⁰ PMPDI-sensitized mesoporous SnO₂.

Photoactivity was recorded for each anode in tested in a scanning voltammetry experiment coupled with light/dark phototransients (Fig. 3a). Working from left to right, the voltage is scanned from -0.2 to +1.0 V vs. Ag/AgCl with a 10 mV s⁻¹ scan rate. For each of the phototransients, illumination of the photoanode causes a rapid rise in anodic (negative y-axis) current and then blocking of the light each 5 s causes the rapid drop in current. The large current spikes observed at ca. +0.1 V vs. Ag/AgCl are also present on bare SnO₂ anodes, indicating that the spikes cannot fully be attributed to PMPDI, but are likely related to SnO2 recombination centers.10,17

We find that by the addition of the 1.3 nm of AlO_x overlayer deposited at 85 °C, SnO₂/PMPDI/AlO_x, significantly increased both peak and steady-state photocurrent by approximately 1.6fold and 2.5-fold, respectively, compared with the system without any AlO_x (Fig. 3a). The increased peak and steady-state photocurrents suggest that the charge carrier production/ collection is increased, likely due to a reduced carrier recombination. Note, the deposition of AlO_r has negligible effect on the absorptance spectrum of the SnO2/PMPDI electrode (Fig. S2†) and alumina itself was shown not to produce significant photocurrent on its own, indicating that AlOx is likely not functioning as a major WOC (Fig. S3†). The addition of AlOx also reduces the ratio of peak to steady-state anodic photocurrent (i.e., current 'spiking' behavior), which is often attributed to charge recombination caused by metal-oxide surface states. 10,17,33-35 The SnO₂/PMPDI system displayed ca. 87% anodic decay from peak to steady-state photocurrent over 5 min at +0.2 V vs. Ag/AgCl, while the SnO₂/PMPDI/AlO_x decayed slightly less, ca. 76%. This spiking behavior can also be indicative of photocorrosion due to excessive charging of the light absorber.36 Photocorrosion is certainly an issue in tough oxidative reactions, such as water splitting, and as such these same experiments were carried out using hydroguinone (H₂Q) (Fig. 4). With the addition of hydroquinone, the spiking behavior is minimized, suggesting that the more kinetically and thermodynamically facile reaction can outrun the recombination pathways. In short, increasing the desirable kinetic pathways with the addition of H₂Q can overcome the recombination pathways. Overall, these observations are consistent with the partial passivation of surface trap states on SnO2 and PMPDI by 1.3 nm thick AlO_x.

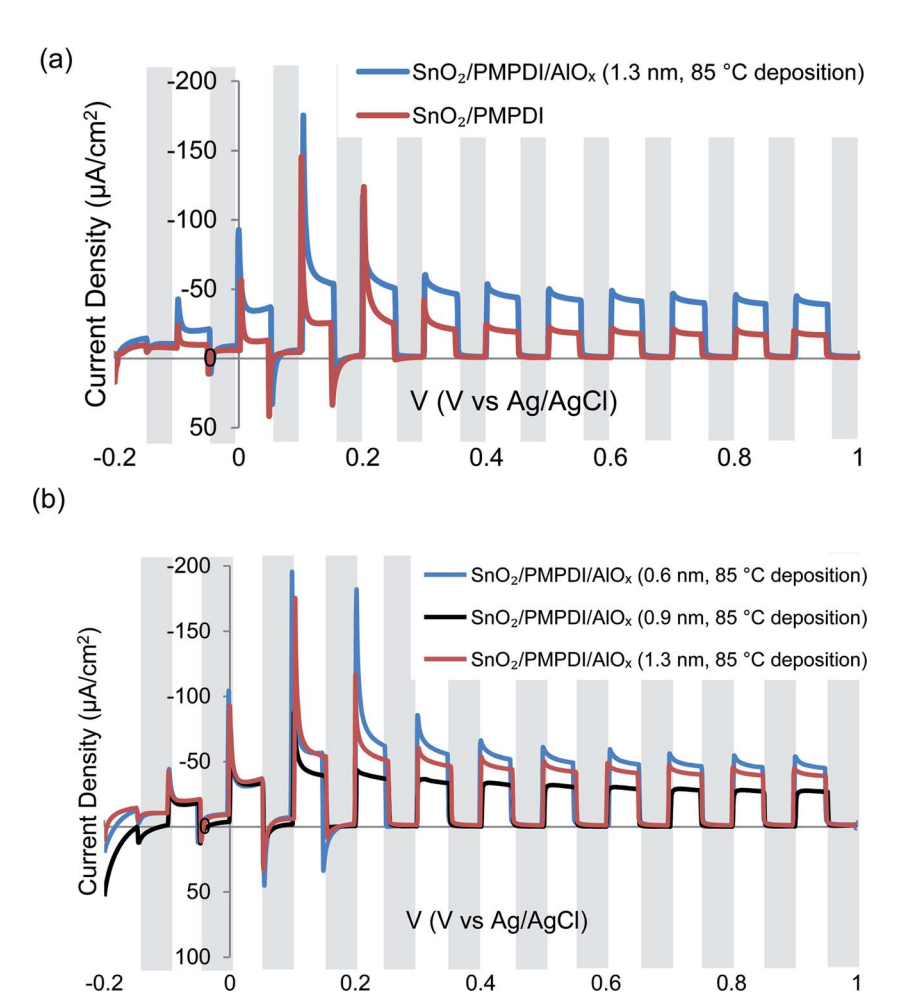


Fig. 3 Photocurrent transients (indicated by light (light-on)/dark (light-off) shading, 5 s each) collected in pH 7, $0.1 \, M$ KPi electrolyte for: (a) SnO₂/ PMPDI/AlO_x (1.3 nm, 85 °C deposition temperature, blue) and SnO₂/PMPDI (red) anodes.; (b) SnO₂/PMPDI/AlO_x (0.6 nm, 85 °C deposition, blue), SnO₂/PMPDI/AlO_x (0.9 nm, 85 °C deposition, black) and SnO₂/PMPDI/AlO_x (1.3 nm, 85 °C deposition, red) anodes. Comparatively thinner, 0.6 nm, layers of alumina yield higher photocurrents than the 0.9 and 1.3 nm counterparts.

To maximize the device performance enhancement by the AlO_r anode passivation layer, it is necessary to optimize the thickness of AlO_x that balances its benefits (e.g., surface state

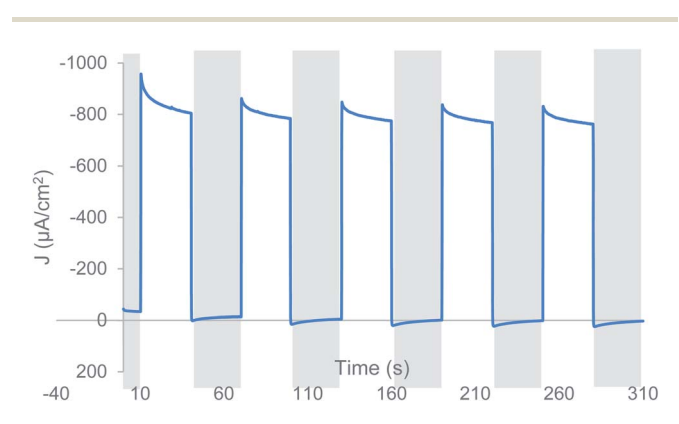


Fig. 4 Photocurrent transients (with 30 s light/dark intervals) for a representative SnO₂/PMPDI/AlO_x/CoO_v (0.6 nm, 85 °C deposition) anode. Transients were performed at +0.2 V vs. Ag/AgCl in pH 7, 0.1 M KPi buffer with 20 mM H₂Q. Background H₂Q currents were subtracted off.

passivation and reduced carrier recombination) with the possible decrease in photoactivity from an ineffective charge transfer between the semiconductor to electrolyte, a decreased surface area, or separation of the dye from the catalyst, all of which can be caused by a too thick AlO_x overlayer. Alumina is an insulator and hence functions as a tunneling barrier. Finding a balance between moving charge carriers through the AlO_x and fully covering the SnO₂ is fundamentally important to minimizing recombination while maintaining charge carrier movement, that is, to optimizing the kinetics. However, there is largely inconsistent information in the literature as to the optimal thickness of ALD overlayer in DS-PEC systems, with reports ranging from sub-monolayer to 3 nm.21,25,28,37-42 Therefore, a series of anodes with varying overlayer thicknesses from 0.6 nm to 1.3 nm were investigated (Fig. 3b) in order to determine the thickness at which the kinetics are optimized, which will be discussed herein and is detailed below in Scheme 1. We find that the photocurrent was maximized with relatively thinner AlO_x layer, reaching, for example, $-182 \mu A cm^{-2}$ at +0.2 V vs. Ag/AgCl for 0.6 nm AlO_x, compared with -64 and $-115 \,\mu\text{A cm}^{-2}$ for 0.9 nm and 1.3 nm thick AlO_x, respectively.

This result illustrates that an even modestly thicker AlO_x passivation layer can indeed interfere with the charge transfer between the anode and electrolyte, consistent with previous literature.43

As illustrated in Fig. 3, we find that the photocurrent spiking behavior still exists regardless of the AlO_x passivation thickness. Considering that photocurrent spiking is often attributed to metal oxide surface trap states, 10,33,35,44 we tested if increasing the AlO_x deposition temperature could affect the spiking behavior, since higher AlO_x ALD temperature should in principle result in the growth of more stoichiometric Al₂O₃ with reduced defect density and increased coating uniformity. 45-51 X-ray photoelectron spectroscopy (XPS) was done in an attempt to detect distinct environments between the alumina depositions, but no differences were observed (Fig. S4†). Specifically, SnO₂/PMPDI anodes were coated with 0.6 nm of AlO_x at 85 °C, 150 °C, and 200 °C, and their photoelectrochemical activities were compared (Fig. 5). Interestingly, the increased AlO_x ALD temperature resulted in a rather minor increase in the extent of photocurrent spiking, while decreasing the overall photocurrent. To quantify the photocurrent spiking behavior, we calculate the percentage of photocurrent decay from peak to steady state measured at +0.2 V vs. Ag/AgCl from each system. The SnO₂/PMPDI/AlO_x systems with AlO_x deposited at 85, 150, and 200 °C displayed a photocurrent decay of ca. 76%, 84%, and 83%, respectively. In the meantime, the photocurrent peak decreased from $-182 \,\mu\text{A cm}^{-2}$ at +0.2 V vs. Ag/AgCl for the AlO_x deposited at 85 $^{\circ}$ C to -107 and $-92 \mu A cm^{-2}$ for the AlO_r deposited at 150 and 200 °C, respectively. However, regardless of deposition temperature, the addition of AlO_x overlayer still yielded a higher photocurrent than the neat PMPDI, consistent with the role of AlO_x mitigating as desired against charge carrier recombination.

A control experiment was performed to show that the decrease in photocurrent at higher AlO_x ALD temperature is not caused by the thermal degradation of PMPDI during ALD. Specifically, thermogravimetric analysis (TGA) confirmed the stability of

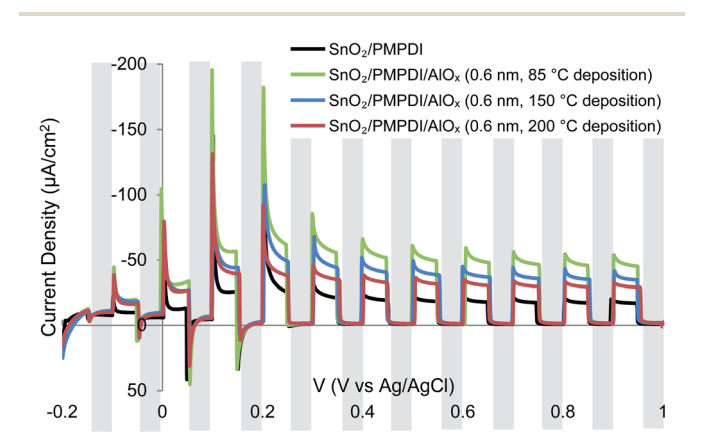


Fig. 5 Photocurrent transients (indicated by light (light-on)/dark (light-off) shading, 5 s each) collected in pH 7, 0.1 M KPi electrolyte for SnO₂/PMPDI (black), SnO₂/PMPDI/AlO_x, (0.6 nm, 85 °C deposition, green), SnO₂/PMPDI/AlO_x, (0.6 nm, 150 °C deposition, light blue), and SnO₂/PMPDI/AlO_x, (0.6 nm, 200 °C deposition, red) anodes. Scans were run from -0.2 to +1.0 V vs. Ag/AgCl. Increasing the deposition temperature of AlOx yielded a decrease in photocurrent.

PMPDI up to 400 °C (Fig. S5†), consistent with the generally reported thermal stability of PDI to approximately 300-600 °C, ¹⁴ so that the ≤200 °C used herein should not be a problem unless there was efficient catalysis of PMPDI decomposition by the deposited AlO_x. This latter possibility was ruled out by a second control experiment demonstrating the unchanged optical absorption spectrum of a photoanode before and after the ALD at the elevated, up to 200 °C temperatures employed (Fig. S2 of the ESI†). The interesting higher photocurrent observed from the AlO_r layer deposited at the lower temperature might be associated with the surface states at AlO_r being able to serve as mediators for the photocatalytic reaction, increasing the overall photocatalytic activity of PMPDI,28,52 an intriguing working hypothesis for going forward and possible further investigation.

In all cases without added catalyst, the photocurrents observed in the SnO₂/PMPDI/AlO_x systems are not attributable to water oxidation, consistent with findings in the original SnO₂/PMPDI system.¹⁰ We hypothesize that perhaps the photocurrent could be due to some combination of dye degradation (though dve losses are minimal and even full dve degradation cannot account for all charge passed),10 oxidation of water to H₂O₂ and oxidation of trace impurities.

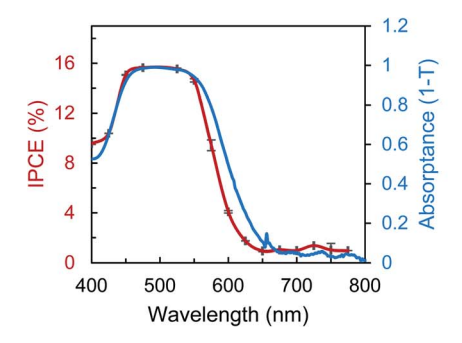
Incident-photon-to-current efficiency (IPCE) and faradaic efficiency of SnO₂/PMPDI/AlO_x photoanodes

The IPCE of the optimized $SnO_2/PMPDI/AlO_x$ (0.6 nm, 85 °C) was measured to examine the role of AlOx layer in improving the photocurrent. An action spectrum of the photocurrent vs. wavelength of incident light was collected in the presence of the two-electron, kinetically facile sacrificial reductant hydroquinone (H₂Q), H₂Q \rightarrow Q²⁻ + 2H⁺ + 2e⁻, Fig. 6, left.

The IPCE spectrum measured with H₂Q resembles the optical absorptance spectrum of PMPDI dye with some deviation at around 400-450 nm, photocurrent presumably due to some direct absorbance of light by bandgap excitation of SnO2.10 By dividing the IPCE by the absorptance of PMPDI, the absorbed photon-tocurrent efficiency (APCE) was calculated, where the APCE is the internal quantum efficiency of the system, that is the combination of the efficiencies of charge transfer across the semiconductorelectrolyte interface times the charge-collection efficiency at the electrode. The observed APCE is \sim 18% for the SnO₂/PMPDI/AlO_r (0.6 nm) (Fig. 6, right), hence modestly superior to those of SnO₂/ PMPDI without AlO_x (APCE = \sim 13%), but \sim 2.5-fold superior to the original thin-film system, indium doped tin oxide (ITO)/ PMPDI with CoO_v WOC (APCE = \sim 6%). The observed, higher APCE indicates that more photocurrent is produced for the given number of absorbed photons when the AlOx overlayer was applied, consistent with the hypothesis discussed: the AlO_x overlayer passivates the defect states at SnO2 surface thereby reducing charge recombination while the surface states of AlOx assist the photocatalytic reaction at the electrolyte interface.

Effects of the combined application of CoO_v WOC and AlO_x passivation layer

We tested if the combination of CoO_y WOC with ALD AlO_x passivation (1.3 nm, 85 °C) could lead to an additional



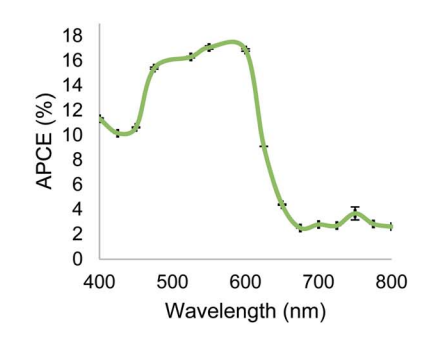


Fig. 6 (Left) IPCE spectrum of $SnO_2/PMPDI/AlO_x$ (0.6 nm, 85 °C deposition) anode in pH 7, 0.1 M KPi buffer with 20 mM H_2Q sacrificial reductant (red) plotted along with the optical absorptance spectrum of PMPDI (blue) and (right) APCE spectra of $SnO_2/PMPDI/AlO_x$ (0.6 nm, 85 °C deposition) anode in pH 7, 0.1 M KPi buffer with 20 mM H_2Q sacrificial reductant.

enhancement in water oxidation photocurrent of the $SnO_2/PMPDI$ photoanode. As discussed above, previous reports have shown that the application of WOC to the DS-PEC system with metal-oxide passivation layer led to an undesired decrease in the photocurrent outputs. 10,21

We find that the photocurrent in our SnO₂/PMPDI/AlO_x/ CoO_v photoanode in fact slightly increased over the SnO₂/ PMPDI/CoO_{ν} control, indicating that the particular AlO_x passivation layer does not interfere with the catalytic function of CoO_v WOC in our case (Fig. 7a). Specifically, we observe that the application of AlO_x increases the magnitude of steady-state photocurrent at a given potential for the system (e.g., from $-15 \mu A cm^{-2}$ to $-19 \mu A cm^{-2}$ at $+0.9 V \nu s$. Ag/AgCl for SnO_2 / PMPDI/CoO_v and SnO₂/PMPDI/AlO_x/CoO_v, respectively), while decreasing the extent of photocurrent spiking (e.g., at +0.2 V vs. Ag/AgCl, 72% decay for SnO₂/PMPDI/AlO_x/CoO_ν and 89% decay for SnO₂/PMPDI/CoO_v), consistent with the reduced charge recombination enabled by AlO_x passivation. An extended experiment looking at photocurrent decay in the optimized SnO₂/PMPDI/AlO_x/CoO_y was also carried out, showing approximately 78% decay in photocurrent after ca. 1.5 hours (Fig. S7†).

To the best of our knowledge, this result represents one of the first observations in which the photoanode passivation does not interfere with the activity of CoO_y WOC as compared to the system without the passivation layer deposited onto a PEC. However, the photocurrent from SnO₂/PMPDI/AlO_x/CoO_y photoanodes is still inferior to those of SnO₂/PMPDI/AlO_x counterparts without CoO_y WOC (Fig. 7a), although the origin of the photocurrent from the latter case is still unknown, given that no catalyst or sacrificial reductant were added and no oxygen detected.

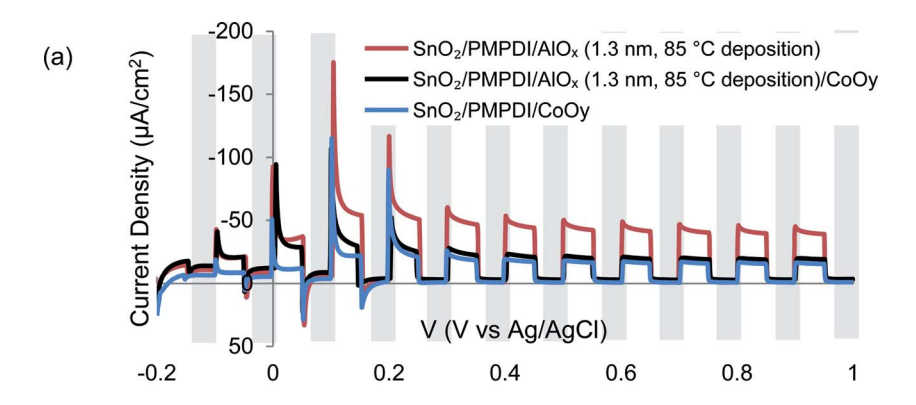
Decreasing the AlO_x thickness in the $SnO_2/PMPDI/AlO_x/CoO_y$ photoanode further increases the photocurrent output (Fig. 7b), similar to the discussed trend in $SnO_2/PMPDI/AlO_x$ without CoO_y WOC. The sample with the thinnest, 0.6 nm AlO_x coating achieved the most photocurrent of $-42~\mu A~cm^{-2}$ at +0.9~V~vs. Ag/AgCl, which is nearly 2.5 times higher than that obtained for $SnO_2/PMPDI/CoO_y$ without any AlO_x overlayer.

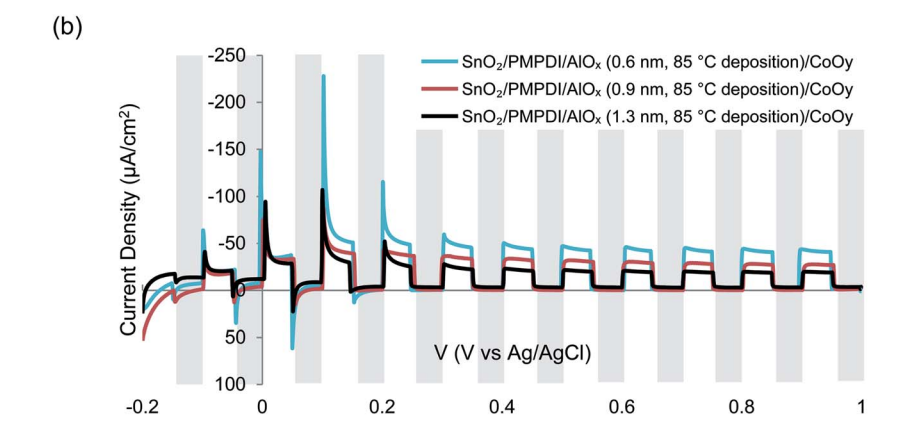
We further demonstrate the observed photocurrent is actually derived from water oxidation by measuring faradic efficiency via the generator-collector (G–C) method^{10,22–24,53} to

detect quantitatively the amount of oxygen produced. We find that for all alumina passivation layer thicknesses, the faradaic efficiency values were largely comparable (Fig. 7c), with the photoanode passivated by 0.6 nm thick alumina displaying a faradaic efficiency of $29 \pm 9\%$. This value is within error of that measured from $SnO_2/PMPDI/CoO_y$ without any AlO_x , and samples with thicker AlO_x showed slightly lower average faradaic efficiencies, though also within error. All samples without catalyst displayed a faradaic efficiency of 0% prior to CoO_y deposition. Of note, photocurrent decays in extended O_2 generation experiments, 20 minutes, resulted in ca. 11% decay in O_2 generation (S8).

We examined the effects of $\mathrm{CoO_y}$ WOC on the V_oc of $\mathrm{SnO_2}/\mathrm{PMPDI/AlO_x}$ photoanode with varying $\mathrm{AlO_x}$ thickness to understand the impact of $\mathrm{CoO_y}$ WOC and $\mathrm{AlO_x}$ on the charge recombination and injection (Fig. 8). When the $\mathrm{SnO_2/PMPDI/AlO_x}$ photoanode is illuminated under open circuit, the measured V_oc reflects the quasi-Fermi energy of electrons ($E_\mathrm{F,n}$) in the nano-SnO₂ substrate with respect to a reference electrode potential. The V_oc is determined by the steady-state charge-carrier concentration—that is, the quasi-equilibrium—set by the balance between the relative rates of the electron injection from the photoexcited dye to $\mathrm{SnO_2}$ vs. the depopulation of the $\mathrm{SnO_2}$ states via recombination 10,54 (see Scheme 1, described in more detail below).

Since the addition of the CoO_v WOC in principle should not alter the electron injection rate from PMPDI, any shift in $V_{\rm oc}$ can be attributed to a change in the recombination rate for a given thickness of AlO_x passivation layer. ^{10,54} Based on the V_{oc} results (Fig. 8 and Table 1), we find a general trend that the measured magnitude of V_{oc} increases while being negative (i.e., the electron quasi-Fermi energy increases due to decreasing rates of recombination relative to injection) as AlO_x thicknesses increases. This result is as expected if AlO_x acts as a tunneling barrier to electrons leaving SnO2. Furthermore, we find a general trend that the measured average V_{oc} is more positive (i.e., the electron quasi-Fermi energy is lower due to increasing rates of recombination relative to injection) after depositing the CoO_{ν} WOC. This result suggests that the CoO_{ν} is able to scavenge electrons from the SnO2, despite the AlOx tunneling barrier, which is consistent with the observed photocurrent





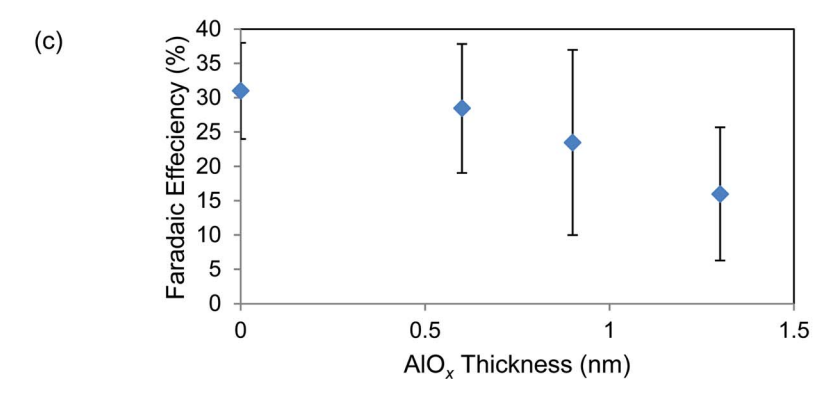


Fig. 7 Photocurrent transients (indicated by light (light-on)/dark (light-off) shading, 5 s each) collected in pH 7, 0.1 M KPi electrolyte for: (a) SnO $_2$ /PMPDI/CoO $_y$ (blue), SnO $_2$ /PMPDI/AlO $_x$ (1.3 nm, 85 °C deposition, red) and SnO $_2$ /PMPDI/AlO $_x$ /CoO $_y$ (1.3 nm, 85 °C deposition, black) anodes; (b) SnO $_2$ /PMPDI/AlO $_x$ /CoO $_y$ (0.6 nm, 85 °C deposition, blue), SnO $_2$ /PMPDI/AlO $_x$ /CoO $_y$ (0.9 nm, 85 °C deposition, red), and SnO $_2$ /PMPDI/AlO $_x$ /CoO $_y$ (1.3 nm, 85 °C deposition, black) anodes; (c) faradaic efficiency values for O $_2$ generation for SnO $_2$ /PMPDI/AlO $_x$ /CoO $_y$ (85 °C AlO $_x$ ALD) with varying AlO $_x$ thicknesses. In all cases oxygen was produced and the faradaic efficiency was found to be the comparable within error.

results, where photocurrents always decreased for a given AlO_x thickness after depositing CoO_y . The samples with 0.9 nm thick AlO_x appear to be outliers from both trends, showing the most positive V_{oc} (most recombination) and negligible effect of CoO_y on V_{oc} within error. The changing kinetics of the system with differing amounts of alumina reflect the complexity of the kinetics herein, both an advantage and disadvantage of adding a component to a system.

A kinetic scheme, Scheme 1, was constructed in order to better illustrate and understand how charge transfer occurs throughout the $SnO_2/PMPDI/AlO_x/CoO_y$ device. Kinetic pathways were identified using k_{trans} , $k_{scavenge}$, k_{inj} , k_{recomb} , k_{abs} , and k_{relax} indicating electron transfer, injection, recombination, absorbance, and relaxation, respectively. This idealized, deliberately minimalistic scheme shows the kinetic pathways for the system in which defects and impurities are not present. The V_{oc}

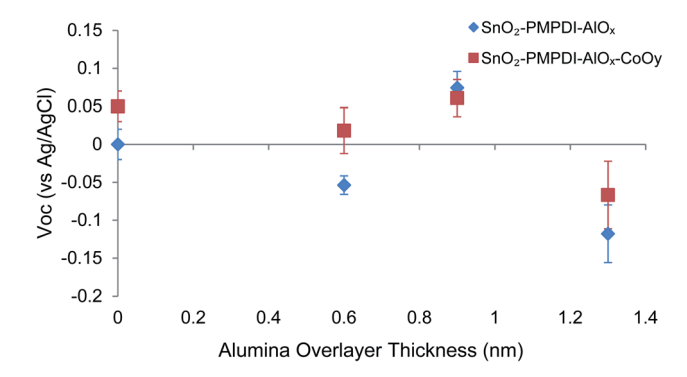


Fig. 8 V_{oc} vs. Ag/AgCl reference electrode in a half-cell setup for SnO₂/PMPDI/AlO_x (85 °C deposition, blue) and SnO₂/PMPDI/AlO_x (85 °C deposition)/CoO_v (red) anodes at differing AlO_x deposition thicknesses. In this case, $V_{oc} \approx E_{F,n}$, the quasi-Fermi energy of electrons in the SnO₂ sub-bandgap states.

Table 1 Open circuit voltage vs. Ag/AgCl for varying thicknesses of alumina deposition with and without CoO_y catalyst addition. The addition of CoO_V either increases V_{oc} (0 nm and 0.6 nm of AlO_X) or induces a negligible change (0.9 nm and 1.3 nm AlO_x)

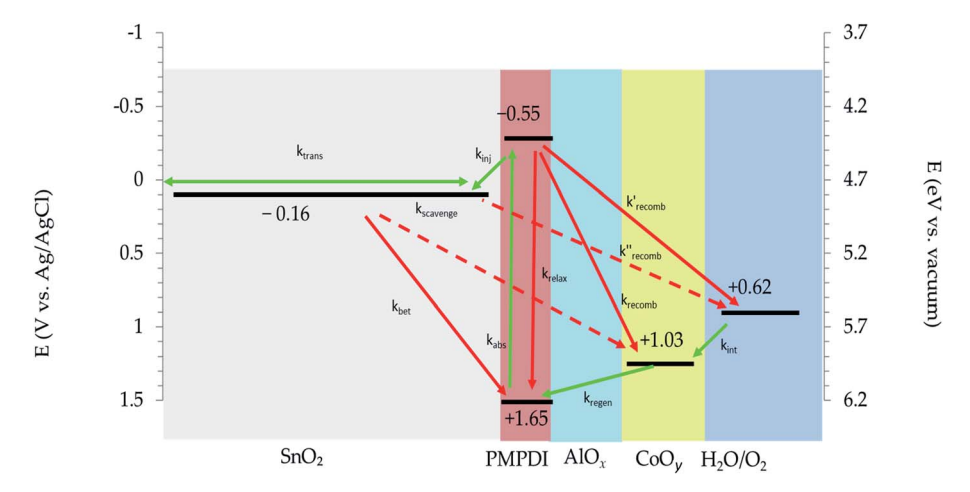
Alumina thickness (nm)	$V_{ m oc}$ without ${ m CoO_y}$ vs. Ag/AgCl	$V_{ m oc}$ with ${ m CoO_y}$ vs. Ag/AgCl
0	0 ± 0.02	0.05 ± 0.02
0.6	-0.054 ± 0.01	$\textbf{0.018} \pm \textbf{0.03}$
0.9	$\textbf{0.074} \pm \textbf{0.02}$	0.061 ± 0.02
1.3	-0.12 ± 0.04	-0.067 ± 0.04

results summarized in Table 1 above can be rationalized by postulating recombination between SnO2 to CoOv, as depicted in Scheme 1 by the red dashed arrow from the SnO₂ conduction band energy level at -0.16 V vs. Ag/AgCl to CoO_{ν} (with a catalytic onset potential of +1.03 V vs. Ag/AgCl).

What is not represented in the kinetic scheme but is crucially important to understanding recombination and efficiency in a WOCatalysis system is the changes in the rate constants for each charge transfer pathway that passes through the AlOx 'blocking' layer. In the case of 1.3 nm thick AlO_x , the V_{oc} is lowest (i.e., most negative), indicating a lowered charge recombination, postulated to be due to a larger tunneling barrier between SnO₂ and CoO_y. Given that 1.3 nm thick AlO_x also results in the lowest amount of photocurrent, this suggests that the comparatively thicker AlO_x passivation layer also slows electron transfer from the CoO_v catalyst to regenerate the photooxidized PMPDI, or slows electron transfer from photo-excited PMPDI to SnO₂. The latter effect is less likely, because the AlOx overlayer was deposited after PMPDI. Hence, while valuable for beginning to understand the present system in better kinetic detail, future studies testing the pathways in Scheme 1 and measuring rate constants will be needed to better understand in detail how and why the addition of the AlO_x layer improves photocurrent in the present system.

Structural model for AlO_x passivation layer and CoO_y WOC

A typical assumption in the dye-sensitized solar cell (DSSC) and DS-PEC literature is that ALD surface treatments are able to uniformly coat the entire interior surface area of a mesoporous metal oxide. However, the AlOx passivation layer prepared by the ALD protocol used in this study is likely unable to produce a fully conformal coating on the PMPDI loaded throughout the bulk of 4 µm-thick mesoporous SnO₂. The ALD process, similar to chemical vapor deposition in nature, relies on an efficient transport of vapor-phase precursors to a target surface on which materials are deposited. Unlike flat substrates, threedimensional (3D) mesoporous substrates require significantly longer time for the precursors to be able to diffuse into the mesopores (i.e., Kundsen diffusion) to generate a fully



Scheme 1 Hypothesized kinetic scheme of the $SnO_2/PMPDI/AIO_x/CoO_v$ system where SnO_2 is grey, PMPDI is pink, AIO_x is blue, and CoO_v is yellow. Green arrows indicate idealized pathways for charge transfer in WOC. Red arrows indicate loss of efficiency in the form of charge-carrier recombination. Arrows to the AlO_X are not included in this scheme based on the assumption that the ultrathin AlO_X is a tunneling barrier in which no charge carrier accumulation occurs. The lack of charge transfer pathways to or from the AlO_x energy states indicates that, qualitatively, the charge transfer pathways of the system with and without AlO_x would be identical; that is, the arrows depicted in a kinetic scheme of the anode would be the same.

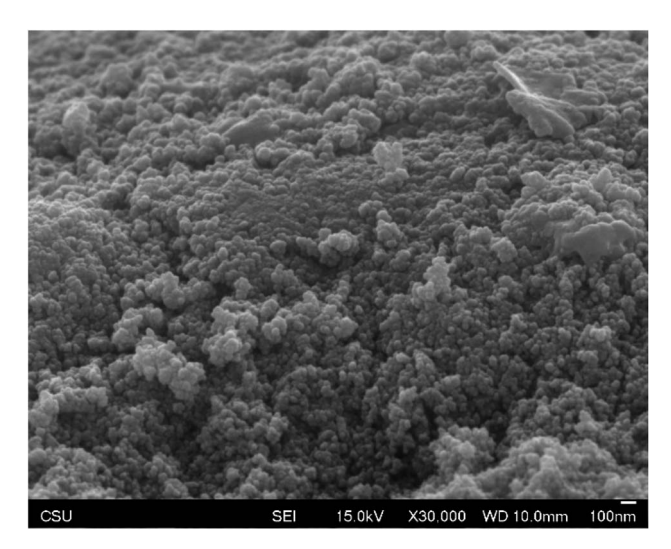


Fig. 9 SEM image of $SnO_2/PMPDI/AIO_x$ (0.6 nm, 85 °C)/CoO_v anode taken at 30 000× magnification.

conformal coating throughout the bulk interior of the mesopores. In our ALD process, the PMPDI-loaded mesoporous SnO₂ was exposed to materials precursors (either TMA or water) for 1 min during each cycle under dynamic vacuum (i.e., continuous evacuation of the chamber under constant flow of background carrier gas (nitrogen; 20 sccm)). That treatment is not expected to allow diffusion of precursors deep into the bulk of mesoporous SnO₂ film. The resulting AlO_x passivation layer should, then and in turn, be covering mostly only the upper portion of mesoporous SnO2 film.

An artistic representation of the SnO₂/PMPDI/AlO_x/CoO_y anode system developed and examined herein was created based on scanning electron microscopy (SEM) imaging of the anodes (Fig. 9). This rendering (Fig. 10) is based on a series of SEM images of the anodes, both with alumina (Fig. 9) and previously published,10 showing the distinctly nanostructured features reflected in this depiction. Understanding the layering

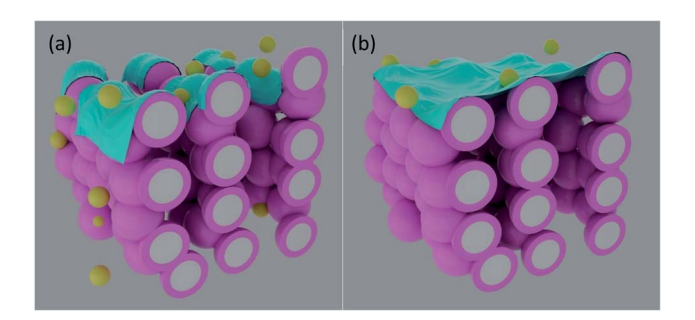


Fig. 10 Idealized structural models of the SnO₂/PMPDI/AlO_x/CoO_v anode with (a) 0-0.9 nm thick AlO_x layer and (b) 1.3 nm thick or greater AlO_x layer, where SnO_2 is grey, PMPDI is pink, AlO_x is blue, and CoO_y is yellow. Note that in (b) a full, impenetrable coverage by the alumina over the SnO₂ surface is implied, and therefore no yellow CoO_v is shown in the lower part of (b). Structural models are based on SEM imaging of anodes, which showed distinct nanostructured behavior as rendered herein.

and interaction of each component is necessary to accurately examine the kinetics of the system as a whole.

For the thinner AlO_v coatings employed, we illustrate a hypothesized thin surface coating at the outer most surface of the SnO₂ only (Fig. 10a). The subsequent application of the CoO_v WOC onto the anode structure likely results in CoO_v directly in contact with PMPDI, and SnO2, within the deeper portion of mesoporous SnO₂ film, as opposed to the CoO_y placed on AlO_x overlayer at the upper region of the SnO₂ film. This is consistent with the observed increased charge recombination and, consequently, reduced photocurrent output for the full system with added CoO_v. Attempts to determine the location and prevalence of cobalt using SEM-energy dispersive X-ray spectrometer (EDS) and XPS were unsuccessful due to the very low, catalytic quantities of CoO_v used (for further discussion see S5 and S7†). Although the CoO_ν catalyst was not visible by XPS, alumina is present in the anodes according to XPS (Fig. S4†).

As for the 1.3 nm-thick AlO_x layer, the passivation now may be thick enough to more thoroughly cover at least some of the mesopores, more similar to Fig. 10b than 10a, preventing at least some direct contact between SnO2 and CoOv as can happen with the ultrathin, 0.6 nm layer for example, so that recombination is not increased (or at least not as much) following the application of CoO_v. But, the thicker AlO_x passivation layer has other effects, as already noted, inhibiting the efficiency of necessary electron transfer from the CoO_v to PMPDI, while also preventing the full utilization of PMPDI loaded within the bulk of mesoporous SnO2 film. The net effect of the even modestly thicker AlO_x layer is that the performance of base SnO₂/PMPDI/ AlO_x , 0.6 nm thickness AlO_x , anode is overall reduced.

Conclusions

In the present study we have examined a SnO₂/PMPDI DS-PEC system for photoelectrochemical water-oxidation catalysis where an ultrathin AlOx passivation layer is added by lowtemperature ALD, with and without a CoO, WOC. The thickness- and deposition-temperature parameters of the ALD were explored with the goal of optimizing the system. The answers obtained to the five primary questions posed at the start of the studies are the following: (i) yes, deposition of an ultrathin alumina overlayer applied by ALD on the PMPDI/SnO2 photoanode can improve the photoactivity and catalytic activity of the system; (ii) yes, perhaps surprisingly as one of the more interesting results of the present study, the addition of specifically a \sim 1 nm-thick AlO_x layer deposited on a 4000 nm (i.e., 4 micron) thick mesoporous anode system can and does have a positive, 2.5-fold improvement in the steady-state photocurrent with 29 \pm 9% faradaic efficiency vs. the control anode without alumina passivation. Reduced charge-carrier recombination explains the observed effect. Next, (iii) yes, layer thickness and deposition temperature of the alumina overlayer are key parameters, a 0.6 nm-thick AlO_x layer deposited at 85 °C providing the best photocatalytic activity in our hands; so that (iv) yes, ALDdeposited, ultrathin AlOx layers is a useful tool to address the carrier recombination in nanostructured/dye systems such as

SnO₂/PMPDI DS-PECs. Additionally, (v) yes, ALD-deposited AlO_x layer does help support the understanding of the "anti-catalysis" of co-depositing a CoO_v WOC on the SnO₂/PMPDI DS-PECs-specifically the picture of direct CoO_v-SnO₂ contactmediated recombination—but was unable to improve the photocurrent in a net SnO₂/PMPDI/AlO_y/CoO_y system. The results document that metal-oxide passivation by lowtemperature ALD can be an effective strategy for improving the water oxidation performance of even nanostructured DS-PECs. The results indicate that further optimizing the ALD protocol by tailoring it towards mesoporous structures—for example, by utilizing the ALD-derived infiltration synthesis method55,56-merits experimental testing.

Overall, we find the addition of an optimized ultrathin AlO_x layer (0.6 nm thick; deposited at 85 °C) improves the SnO₂/ PMPDI/AlO_x system's photoactivity by a factor of up to \sim 3-fold with reduced recombination. However, the addition of CoO_v still results in a decrease in photoactivity compared to the SnO₂/ PMPDI/AlO_x system without CoO_y, but a faradaic efficiency of oxygen production of ca. 30%. We attribute the lack of a performance enhancement by CoO_{ν} WOC to incomplete coverage of each SnO₂ nanoparticle by the AlO_x. Despite the decrease in photoactivity with the addition of the CoO_v WOC, the SnO₂/PMPDI/AlO_x/CoO_v system yields a higher photocurrent in all cases compared to the original, alumina-free SnO₂/ PMPDI/CoO_ν system.

Conflicts of interest

There are no conflicts to declare.

Acknowledgements

This research was supported by the National Science Foundation under Grant No. 1664646. The authors thank the members of Prof. Finke's research group and Dr Joel Kirner for reading draft versions of this manuscript and providing valuable feedback. Additional thanks to Audrey Jewell for production of artistic renderings. This research used resources of the Center for Functional Nanomaterials, which is a U.S. DOE Office of Science Facility, at Brookhaven National Laboratory under Contract No. DE-SC0012704.

References

- 1 R. E. Smalley, Future Global Energy Prosperity: The Terawatt Challenge, Mater. Matters, 2004, 30, 412-417.
- 2 N. S. Lewis and D. G. Nocera, Powering the Planet: Chemical Challenges in Solar Energy Utilization, Proc. Natl. Acad. Sci. U. S. A., 2006, 103, 15729-15735.
- 3 A. Kudo and Y. Miseki, Heterogeneous Photocatalyst Materials for Water Splitting, Chem. Soc. Rev., 2009, 38, 253-278.
- 4 J. T. Kirner and R. G. Finke, Water-Oxidation Photoanodes Using Organic Light- Harvesting Materials: A Review, J. Mater. Chem. A, 2017, 5, 19560-19592.

- 5 Y. Tachibana, L. Vayssieres and J. R. Durrant, Artificial Photosynthesis for Solar Water-Splitting, Nat. Photonics, 2012, 6, 511-518.
- 6 J. R. Swierk and T. E. Mallouk, Design and Development of Photoanodes for Water-Splitting Dye-Sensitized Photoelectrochemical Cells, Chem. Soc. Rev., 2013, 42, 2357-2387.
- 7 I. Roger, M. A. Shipman and M. D. Symes, Earth-Abundant Catalysts for Electrochemical and Photoelectrochemical Water Splitting, Nat. Rev. Chem., 2017, 1, 1-14.
- 8 K. Y. Law, Organic Photoconductive Materials: Recent Trends and Developments, Chem. Rev., 1993, 93, 449-486.
- 9 J. T. Kirner, J. J. Stracke, B. A. Gregg and R. G. Finke, Visible-Light-Assisted Photoelectrochemical Water Oxidation by Thin Films of a Phosphonate-Functionalized Pervlene Diimide Plus CoO_x Cocatalyst, ACS Appl. Mater. Interfaces, 2014, 6, 13367-13377.
- 10 J. T. Kirner and R. G. Finke, Sensitization of Nanocrystalline Metal Oxides with a Phosphonate- Functionalized Perylene Diimide for Photoelectrochemical Water Oxidation with a CoO_x Catalyst, ACS Appl. Mater. Interfaces, 2017, 9, 27625-27637.
- 11 N. Mariotti, M. Bonomo, L. Fagiolari, N. Barbero, C. Gerbaldi, F. Bella and C. Barolo, Recent Advances in and Cost-Effective Materials Sustainable Dye-Sensitized Solar Cells, Green Chem., 2020, 22, 7168-7218.
- 12 A. Carella, F. Borbone and R. Centore, Research Progress on Photosensitizers for DSSC, Front. Chem., 2018, 6, 481.
- Shalini, R. Balasundaraprabhu, T. S. N. Prabavathy, S. Senthilarasu and S. Prasanna, Status and Outlook of Sensitizers/Dyes Used in Dye Sensitized Solar Cells (DSSC): A Review, Int. J. Energy Res., 2016, 40, 1303-1320.
- 14 N. Pasaogullari, H. Icil and M. Demuth, Symmetrical and Unsymmetrical Perylene Diimides: Their Synthesis, Photophysical and Electrochemical Properties, Dyes Pigm., 2006, 69, 118-127.
- 15 A. J. Bard, G. M. Whitesides, R. N. Zare and F. W. McLafferty, Holy Grails in Chemistry, Acc. Chem. Res., 1995, 28, 91.
- 16 M. W. Kanan and D. G. Nocera, In Situ Formation of an Oxygen-Evolving Catalyst in Neutral Water Containing Phosphate and Co²⁺, Science, 2008, 321, 1072-1073.
- 17 C. Prasittichai and J. T. Hupp, Surface Modification of SnO₂ Photoelectrodes in Dye-Sensitized Solar Cells: Significant Improvements in Photovoltage via Al₂O₃ Atomic Layer Deposition, J. Phys. Chem. Lett., 2010, 1, 1611-1615.
- 18 J. R. Swierk, N. S. McCool, T. P. Saunders, G. D. Barber and T. E. Mallouk, Effects of Electron Trapping and Protonation on the Efficiency of Water-Splitting Dye-Sensitized Solar Cells, J. Am. Chem. Soc., 2014, 136, 10974-10982.
- 19 N. S. Foundation. Catalytic Chemistry Workshop on Defining Critical Directions for the Future; 2011; pp. 1-20.
- Kay and M. Grätzel, Dye-Sensitized Core-Shell Nanocrystals: Improved Efficiency of Mesoporous Tin

- Oxide Electrodes Coated with a Thin Layer of an Insulating Oxide, *Chem. Mater.*, 2002, **14**, 2930–2935.
- 21 R. J. Kamire, K. L. Materna, W. L. Hoffeditz, B. T. Phelan, J. M. Thomsen, O. K. Farha, J. T. Hupp, G. W. Brudvig and M. R. Wasielewski, Photodriven Oxidation of Surface-Bound Iridium-Based Molecular Water-Oxidation Catalysts on Perylene-3,4-Dicarboximide-Sensitized TiO₂ Electrodes Protected by an Al₂O₃ Layer, *J. Phys. Chem. C*, 2017, 121, 3752–3764.
- 22 Y. Zhao, J. R. Swierk, J. D. Megiatto Jr, B. Sherman, W. J. Youngblood, D. Qin, D. M. Lentz, A. L. Moore, T. A. Moore, D. Gust and T. E. Mallouk, Improving the Efficiency of Water Splitting in Dye-Sensitized Solar Cells by Using a Biomimetic Electron Transfer Mediator, *Proc. Natl. Acad. Sci. U. S. A.*, 2012, 109, 15612–15616.
- 23 D. L. Ashford, B. D. Sherman, R. A. Binstead, J. L. Templeton and T. J. Meyer, Electro-Assembly of a Chromophore-Catalyst Bilayer for Water Oxidation and Photocatalytic Water Splitting, *Angew. Chem., Int. Ed.*, 2015, 54, 4778–4781.
- 24 B. D. Sherman, M. V. Sheridan, C. J. Dares and T. J. Meyer, Two Electrode Collector—Generator Method for the Detection of Electrochemically or Photoelectrochemically Produced O₂, Anal. Chem., 2016, 88, 7076–7082.
- 25 K. Hanson, M. D. Losego, B. Kalanyan, G. N. Parsons and T. J. Meyer, Stabilizing Small Molecules on Metal Oxide Surfaces Using Atomic Layer Deposition, *Nano Lett.*, 2013, 13, 4802–4809.
- 26 M. E. Donders, H. C. M. Knoops, M. C. M. Van De Sanden, W. M. M. Kessels, P. H. L. Notten and M. E. Donders, Remote Plasma Atomic Layer Deposition of Co₃O₄ Thin Films, J. Electrochem. Soc., 2011, 158, 92–96.
- 27 J. P. Klesko, M. M. Kerrigan and C. H. Winter, Low Temperature Thermal Atomic Layer Deposition of Cobalt Metal Films, *Chem. Mater.*, 2016, **28**, 700–703.
- 28 L. Wang, D. Yan, X. Ye, M. Liu and C.-Y. Nam, Improved Stability and Performance of Visible Photoelectrochemical Water Splitting on Solution- Processed Organic Semiconductor Thin Films by Ultrathin Metal Oxide Passivation, Chem. Mater., 2018, 30, 324–335.
- 29 M. K. Brennaman, R. J. Dillon, L. Alibabaei, M. K. Gish, C. J. Dares, D. L. Ashford, R. L. House, G. J. Meyer, J. M. Papanikolas and T. J. Meyer, Finding the Way to Solar Fuels with Dye-Sensitized Photoelectrosynthesis Cells, J. Am. Chem. Soc., 2016, 138, 13085–13102.
- 30 N. S. Mccool, J. R. Swierk, C. T. Nemes, T. P. Saunders, C. A. Schmuttenmaer and T. E. Mallouk, Proton-Induced Trap States, Injection and Recombination Dynamics in Water-Splitting Dye-Sensitized Photoelectrochemical Cells, ACS Appl. Mater. Interfaces, 2016, 8, 16727–16735.
- 31 R. Zazpe, J. Prikryl, V. Gä, K. Nechvilova, L. Benes, L. Strizik, J. Ales, M. Bosund, H. Sopha and J. M. Macak, Atomic Layer Deposition Al₂O₃ Coatings Significantly Improve Thermal, Chemical, and Mechanical Stability of Anodic TiO2 Nanotube Layers, *Langmuir*, 2017, 33, 3208–3216.
- 32 P. Xu, N. S. Mccool and T. E. Mallouk, Water Splitting Dye-Sensitized Solar Cells, *Nano Today*, 2017, **14**, 42–58.

- 33 J. Vandermolen, W. Gomes and F. Cardon, Investigation on the Kinetics of Electroreduction, *J. Electrochem. Soc.*, 1980, **10**, 2650–2651.
- 34 P. Salvador and C. Gutierrez, Mechanisms of Charge Transfer at the Semiconductor-Electrolyte Interface, *J. Electrochem. Soc.*, 1984, **131**, 326–336.
- 35 J. W. Ondersma and T. W. Hamann, Measurements and Modeling of Recombination from Nanoparticle TiO₂ Electrodes, *J. Am. Chem. Soc.*, 2011, **133**, 8264–8271.
- 36 B. Weng, M.-Y. Qi, C. Han, Z.-R. Tang and Y.-J. Xu, Photocorrosion Inhibition of Semiconductor-Based Photocatalysts: Basic Principle, Current Development, and Future Perspective, *ACS Catal.*, 2019, **9**, 4642–4687.
- 37 R. J. Kamire, M. B. Majewski, W. L. Hoffeditz, B. T. Phelan, O. K. Farha, J. T. Hupp and M. R. Wasielewski, Photodriven Hydrogen Evolution by Molecular Catalysts Using Al₂O₃-Protected Perylene-3,4-Dicarboximide on NiO Electrodes: The Design of Efficient Hydrogen-Evolving Photocathodes for Dye-Sensitized Photoelectrochemical Cells, *Chem. Sci.*, 2017, 8, 541–549.
- 38 H.-J. Son, C. Prasittichai, J. E. Mondloch, L. Luo, J. Wu, D. W. Kim, O. K. Farha and J. T. Hupp, Dye Stabilization and Enhanced Photoelectrode Wettability in Water-Based Dye-Sensitized Solar Cells through Post-Assembly Atomic Layer Deposition of TiO₂, *J. Am. Chem. Soc.*, 2013, 135, 11529–11532.
- 39 K. E. Michaux, A. A. Gambardella, L. Alibabaei, D. L. Ashford, B. D. Sherman, R. A. Binstead, T. J. Meyer and R. W. Murray, Visible Photoelectrochemical Water Splitting Based on a Ru(II) Polypyridyl Chromophore and Iridium Oxide Nanoparticle Catalyst, *J. Phys. Chem. C*, 2015, **119**, 17023–17027.
- 40 A. M. Lapides, B. D. Sherman, M. K. Brennaman, C. J. Dares, K. R. Skinner, J. L. Templeton and T. Meyer, J. Synthesis, Characterization, and Water Oxidation by a Molecular Chromophore-Catalyst Assembly Prepared by Atomic Layer Deposition. The "Mummy" Strategy, *Chem. Sci.*, 2015, 6, 6398–6406.
- 41 N. Kaeffer, J. Massin, C. Lebrun, O. Renault, M. Chavarot-Kerlidou and V. Artero, Covalent Design for Dye-Sensitized H₂-Evolving Photocathodes Based on a Cobalt Diimine– Dioxime Catalyst, *J. Am. Chem. Soc.*, 2016, **138**, 12308–12311.
- 42 T. W. Hamann, O. K. Farha and J. T. Hupp, Outer-Sphere Redox Couples as Shuttles in Dye-Sensitized Solar Cells. Performance Enhancement Based on Photoelectrode Modification via Atomic Layer Deposition, *J. Phys. Chem. C*, 2008, **112**, 19756–19764.
- 43 J. Guo, C. She and T. Lian, Effect of Insulating Oxide Overlayers on Electron Injection Dynamics in Dye-Sensitized Nanocrystalline Thin Films, *J. Phys. Chem. C*, 2007, **111**, 8979–8987.
- 44 T. C. Li, M. S. Góes, F. Fabregat-Santiago, J. Bisquert, P. R. Bueno, C. Prasittichai, J. T. Hupp and T. J. Marks, Surface Passivation of Nanoporous TiO₂ via Atomic Layer Deposition of ZrO₂ for Solid-State Dye-Sensitized Solar Cell Applications, J. Phys. Chem. C, 2009, 113, 18385–18390.

- 45 N. Batra, J. Gope, J. Panigrahi, R. Singh and P. K. Singh, Influence of Deposition Temperature of Thermal ALD Deposited Al₂O₃ Films on Silicon Surface Passivation, AIP Adv., 2015, 5, 67113.
- 46 G. Dingemans, M. C. M. van de Sanden and W. M. M. Kessels, Influence of the Deposition Temperature on the C-Si Surface Passivation by Al₂O₃ Films Synthesized by ALD and PECVD, Electrochem. Solid-State Lett., 2010, 13, H76-H79.
- 47 K. Kukli, M. Ritala, M. Leskelä and J. Jokinen, Atomic Layer Epitaxy Growth of Aluminum Oxide Thin Films from a Novel Al(CH₃)₂Cl Precursor and H₂O, J. Vac. Sci. Technol., A, 1997, **15**, 2214-2218.
- 48 N. Batra, J. Gope, R. Singh, J. Panigrahi, S. Tyagi, P. Pathi, S. K. Srivastava, C. M. S Rauthan and P. K. Singh, Effect of Low Thermal Budget Annealing on Surface Passivation of Silicon by ALD Based Aluminum Oxide Films, Phys. Chem. Chem. Phys., 2014, 16, 21804-21811.
- 49 J. M. Rafí, M. Zabala, O. Beldarrain and F. Campabadal, Deposition Temperature and Thermal Annealing Effects on the Electrical Characteristics of Atomic Layer Deposited Al₂O₃ Films on Silicon, J. Electrochem. Soc., 2011, 158, G108-G114.
- 50 M. D. Groner, F. H. Fabreguette, J. W. Elam and S. M. George, Low-Temperature Al₂O₃ Atomic Layer Deposition, Chem. Mater., 2004, 16, 639-645.

- 51 V. Naumann, M. Otto, R. B. Wehrspohn, M. Werner and C. Hagendorf, Interface and Material Characterization of Thin ALD-Al₂O₃ Layers on Crystalline Silicon, Energy Procedia, 2012, 27, 312-318.
- 52 S. R. James Durrant, S. Corby, L. Francas, A. Kafizas and J. R. Durrant, Determining the Role of Oxygen Vacancies in the Photoelectrocatalytic Performance of WO3 for Water Oxidation Determining the Role of Oxygen Vacancies in the Photoelectrocatalytic Performance of WO 3 for Water Oxidation, Chem. Sci., 2020, 11, 2907-2914.
- 53 B. D. Sherman, M. V. Sheridan, K.-R. Wee, N. Song, C. J. Dares, Z. Fang, Y. Tamaki, A. Nayak and T. J. Meyer, Analysis of Homogeneous Water Oxidation Catalysis with Collector-Generator Cells, Inorg. Chem., 2015, 55, 512-517.
- 54 S. Ardo and G. J. Meyer, Photodriven Heterogeneous Charge Transfer with Transition-Metal Compounds Anchored to TiO₂ Semiconductor Surfaces, Chem. Soc. Rev., 2009, 38, 115-164.
- 55 A. Subramanian, N. Tiwale and C. Y. Nam, Review of Recent Advances in Applications of Vapor-Phase Material Infiltration Based on Atomic Layer Deposition, JOM, 2019, 71, 185-196.
- 56 E. K. McGuinness, F. Zhang, Y. Ma, R. P. Lively and M. D. Losego, Vapor Phase Infiltration of Metal Oxides into Nanoporous Polymers for Organic Solvent Separation Membranes, Chem. Mater., 2019, 31, 5509-5518.